JOURNAL OF OPTOELECTRONICS AND ADVANCED MATERIALS, Vol. 11, No. 11, November 2009, p. 1637 - 1640

Zinc oxide nanorods on porous silicon/silicon substrates

L. S. CHUAH*, Z. HASSAN, S. S. TNEH
Nano-Optoelectronics Research and Technology Laboratory, School of Physics, Universiti Sains Malaysia, 11800 Minden, Penang, Malaysia

Zinc thin films were deposited onto porous silicon (PSi) substrates by dc sputtering using a Zn target. These films were then annealed under flowing (6 L min^{-1}) oxygen gas environment in the furnace at 600 ºC for 2 hours. Porous silicon is used as an intermediate layer between silicon and ZnO films and it provides a large area composed of an array of voids. The PSi samples were prepared using photoelectrochemical method on n-type silicon wafer with (111) and (100) orientation. To prepare porous structures, the samples were dipped into a mixture of HF:Ethanol (1:1) for 5 minutes with current densities of 50 mA/cm^2, and subjected to external illumination with a 500W UV lamp. The surface morphology and the nanorods structure of the ZnO films were characterized by scanning electron microscope (SEM) and high resolution X-ray diffraction (HR-XRD). We synthesized the ZnO nanorods with diameter of 80-100 nm without any catalysts or templates. XRD pattern confirmed that the ZnO nanorods were of polycrystalline structure in nature with a hexagonal close packed lattice and c-axis oriented perpendicular to the substrate surface.

(Received October 12, 2009; accepted November 12, 2009)

Keywords: Porous silicon, ZnO, Sputtering, SEM, XRD

1. Introduction

Zinc oxide (ZnO) films with a direct wide band gap (3.37 eV) semiconductor with a large excitonic binding energy (60 meV) at room temperature (RT) are very attractive materials for applying them to devices such as light-emitting diodes (LEDs) and laser diodes in near UV region [1–3]. Low dimensional structures of ZnO (wires, rods, belts, tubes and whiskers) are now under intensive investigations for exceptional electronic, optical, chemical and mechanical properties [4–7]. A good optoelectronic device should not only have high luminous efficiency, high thermo-stability and low threshold of luminescence, but also can be tuned effectively and easily. Intrinsic ZnO nanorods have been observed to emit radiation in the UV and visible spectral region at room temperature. The visible emission of ZnO is usually ascribed to structural defects [8-10].

ZnO is noteworthy for the ease with which it forms one dimensional nanostructures (nanobelts, nanowires, nanorods, nanotubes). The high aspect ratios, size effects and possible quantum confinement effects presented by such nanostructures offer many potential advantages, for example, improved sensitivity to chemical agents and much enhanced luminescence efficiency.

Crystallinity and orientation play a very important role in the optoelectronic properties of the ZnO films. The degree of orientation is influenced by growth conditions such as temperature, background gas composition and pressure and particle energy [11]. A broad variety of techniques have been used for the deposition of nano ZnO films, such as metalorganic chemical vapor deposition [12], sol–gel method [13], hydrothermal growth [14], thermal evaporation and pulsed laser deposition [15]. In most studies, ZnO nanostructures are grown on sapphire substrates. Due to the same hexagonal type lattice structure. Compared with sapphire, silicon substrates are cheaper and available in large size. Thermal expansion coefficient of Si (3.57 x 10^{-6} $ºC^{-1}$) [16] is very close to that of ZnO (4.0 x 10^{-6} $ºC^{-1}$) [16]. However, lattice mismatch between Si and ZnO is large.

In the last decade, porous semiconductors [17] have been widely studied, primarily due to the potential for intentional engineering of properties not readily obtained in the corresponding crystalline precursors as well as the potential applications in optoelectronics, chemical and biochemical sensing [18]. When porosity is formed, these materials exhibit various special optical features, fro instances, the shift of bandgap [19], luminescence intensity enhancement [20], as well as photoresponse improvement [21]. Among porous semiconductors, porous silicon (PSi) [22] is a material creating great scientific and technological interest because of its ample range of application; it has recently been used as growth template for epitaxial re-growth; this could reduce the density of structural defects significantly and allows the growth of residual free epitaxial ZnO layers.

In this field, to the best of our knowledge, this is the first time that porous silicon (PSi) layer was used as an intermediate buffer layer between Si wafer and ZnO. The PSi provides a large area composed of an array of voids and interconnected clusters or rods. This sponge-like structure will limit strain and cracks development after the post growth cooling. In this work, we report results of ZnO nanorods grown on porous silicon. The surface morphology and the crystalline structure of the ZnO nanorods were characterized by scanning electron microscope (SEM) and X-ray diffraction (XRD) at room temperature.

2. Experimental

Prior to the dc sputtering deposition, the porous samples were prepared using photoelectrochemical (PEC) method on n-type silicon wafer with (111) and (100) orientation. Before electrochemical etching, RCA

chemical cleaning was applied. The chemical etching reveals atomic terraces and passivates silicon surface atoms by hydrogen atoms (H-termination). To prepare porous structures, the samples were dipped into a mixture of HF-C_2H_5OH electrolyte (with volume ration of 1:1) for 5 minutes with current densities of 50 mA/cm^2. Due to the hydrophobic character of clean silicon surface, the C_2H_5OH is necessary to improve the wettability of porous silicon.

Samples were illuminated with 500W UV lamp and subsequently well rinsed in de-ionized water. The anodization is performed in potentiostatic mode. Typical PEC wet etching apparatus is schematically shown in Fig. 1. In electrochemical setup, silicon was the anode, Pt was the counter electrode. Zn films were deposited by dc sputtering deposition technology from high purity Zn targets with a purity of 99.99 %. Subsequent, the Zn films were then annealed under flowing (6 L min^{-1}) oxygen gas environment in the furnace at 600 ºC for 2 hours. The growth conditions for ZnO films are summarized in Table 1.

Table 1. Sputtering condition for Zn deposition.

Target	zinc (99.99 %)
Target diameter	3 inch
Target-substrates distances	~ 10 cm
Substrate	Porous silicon
Residual pressure	< 5 x 10^{-5} Torr
Gas	Ar 99.999 %
Sputtering pressure	4.0 x 10^{-3} Torr
Substrate temperature	Room temperature (~ 25 °C)
Deposition time	7.5 min

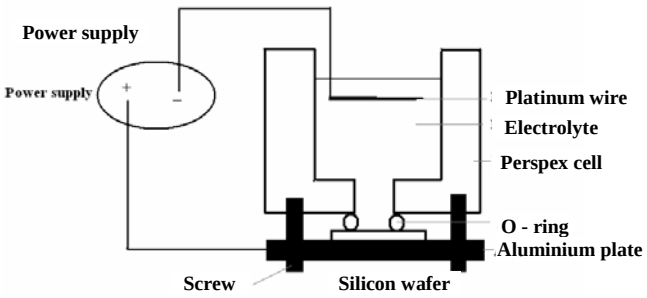

Fig. 1. Schematic of photoelectrochemical (PEC) wet etching apparatus.

The thickness of ZnO film was determined by a surface step profile analyzer. Structural characterization using scanning electron microscope (SEM) (JOEL JSM-6460LV) and X-ray diffraction (XRD) (PANalytical X'pert PRO MRD) were carried out. The carrier concentration and mobility were measured by Hall Effect.

3. Results and discussion

Fig. 2 presents the plan view SEM micrographs of PSi prepared on n-Si. For porous Si(111) substrate, in the plan-view the rigid triangular shaped macroarray network of 300 – 400 nm sizes is clearly seen. The characteristic faceted, triangular shaped pores illustrate an orientation dependence of the photo anodization process of the Si(111) material, probably due to the anisotropy of Si(111) dissolution. For porous Si(100) substrate, pores formed by the rigid circular shaped network with diameter up to 400 nm are clearly seen in the plan view SEM image. The thickness for porous (111) and (100) orientation were around 0.5 μm and 1 μm.

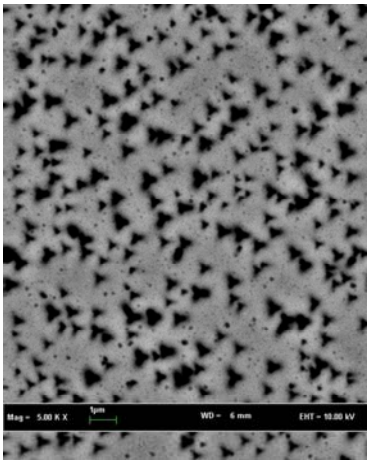

a

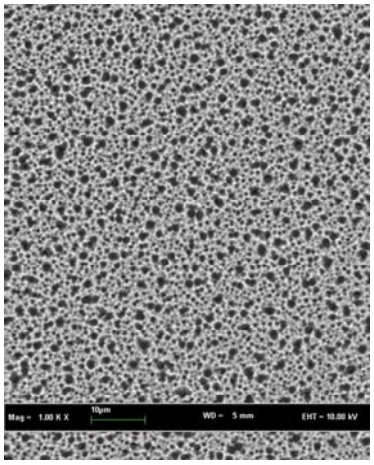

b

Fig. 2. SEM images of porous silicon layers on (a) Si(111); and (b) Si(100) substrates by PEC-etching.

During anodic etching, the material between pores was generally depleted of carriers, and the presence of a depletion layer is responsible for current localization at pore tips. After reaching a critical thickness, pore walls are devoid of holes and hence inert to lateral anodic etching [23]. But the etching rate of the Si(100) crystal plane is about two orders of magnitude larger than that of the (111) crystal plane. The use of a porous layer is also a good alternative in lattice mismatch heteroepitaxy. The PSi layer is obtained on the Si substrate. Its skeleton is supple, thus reducing the stress induced at the cooling phase and limiting the formation of dislocation and cracks in ZnO layers.

The samples obtained were semi-transparent and dark pink in color. Fig. 3 shows the plan view SEM images of ZnO nanorods on porous Si(111) and Si(100) substrates.

It can be seen that the layer consists of agglomerated nanorods. We synthesized 80-100 nm diameter ZnO nanorods without any catalysts or templates. The shape is a consequence of lattice-mismatched materials where the nucleation of the film is initiated on protruding crystals on the rough underlying substrate. SEM has been used to understand the effects of the substrate on crystalline properties of the samples. The results indicated that the porous silicon substrate is beneficial to improve the crystalline quality in lattice mismatch heteroepitaxy due to its sponge-like structure. The thickness of the ZnO cross section from the SEM image are about 301 nm which is in good agreement with the thickness determined by a surface step profile analyzer which is about 290 nm.

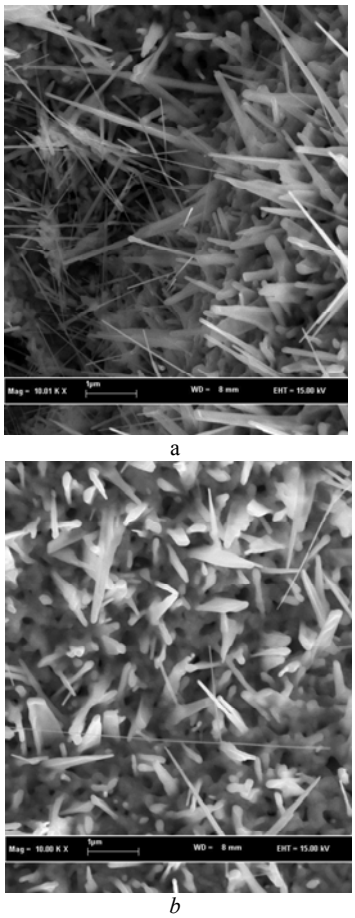

a

b

Fig. 3. SEM images of ZnO grown on porous (a) Si(111) and (b) Si(100) substrates.

The unintentionally doped ZnO exhibited n-type conductivity. This has long been attributed to oxygen vacancies. Such oxygen deficiency could arise from the low dissociation energy of the zinc-oxygen bond. From the Hall measurements, the Hall mobility and electron concentration of the resulting unintentionally doped ZnO are about (150-200) cm^2/Vs and (5-7) x 10^{17} cm^{-3}, respectively.

Energy dispersive X-ray (EDX) analysis (in the SEM) was used to test the composition of nanorods. Fig. 4 shows one such spectrum, for the case of ZnO nanorods. Zinc and oxygen are the only detectable elements, supporting the view that no other metal elements are aiding in catalyzing the observed nanorod growth. Thus we conclude that the rods and, in this case, the capping particles, must be ZnO without defects or dislocations.

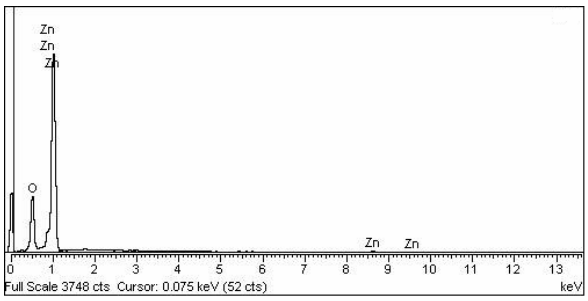

Fig. 4. EDX spectrum from a sample of nanorods grown for 600 ºC for 2 hours on a bare porous Si substrate.

X-ray diffraction is performed to investigate the crystal phase of the studied samples. Figs. 5(a) and (b) represent typical X-ray diffraction (XRD) profile of the ZnO nanorods grown on the porous silicon substrates. For Fig. 5(a), the peak from wurtzite ZnO and metallic Zn plane are observed apart from the (111) peak from the porous silicon substrate. For Fig. 5(b), the peak located at around 69.4° is attributed to the Si (400) planes. XRD pattern confirmed that the ZnO nanorods were of polycrystalline structure in nature with a hexagonal close packed lattice and c-axis oriented perpendicular to the substrate surface.

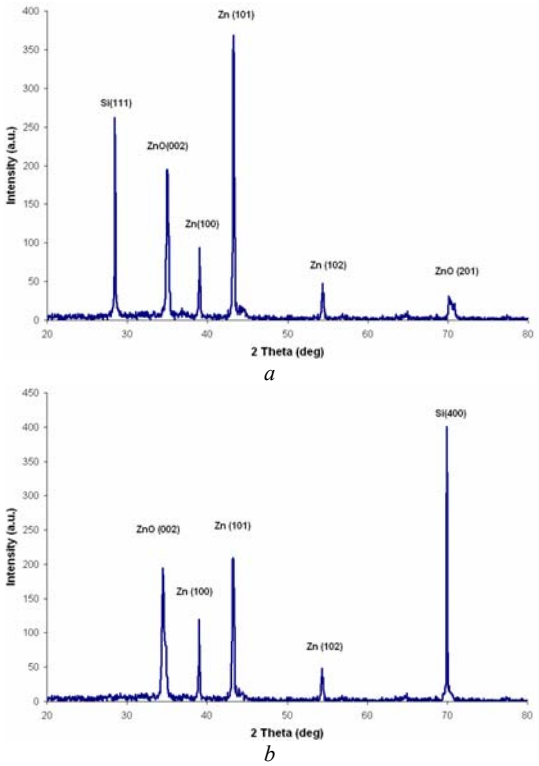

Fig. 5. XRD phase analysis scan of ZnO grown on porous (a) Si(111); and (b) Si(100) substrates.

We have calculated the particle size (D) from the full width at half maximum value for the prominent (0 0 2) peaks using the Scherrer formula, $D = 0.94\lambda/\beta \cos\theta$, where λ is the wavelength of the Kα characteristic X-ray and θ is the diffraction (Bragg) angle. Structural analysis revealed polycrystalline structure with crystallite size of 44 ± 0.05nm and 30 ± 0.05nm for ZnO films grown on Si(1 1 1) and Si(1 0 0) orientation, respectively. This indicates that the films deposited at porous Si(111) are expected to have the best crystallinity.

4. Conclusions

In this work, a simple method was developed to synthesize ZnO nanorods on PSi(111) and PSi(100) substrates. ZnO nanorod are successfully fabricated in a substrate-free manner by annealing process at a growth temperature of 600 ◦C. We have used SEM, XRD, PL and Raman scattering to characterize the samples. From the Hall measurements, the resulting unintentionally doped ZnO nanorods have Hall mobility and electron concentration of about (150-200) cm^2/Vs and (5-7) x 10^{17} cm^{-3}, respectively. Structural analysis revealed polycrystalline structure with crystallite size of 44 ± 0.05nm and 30 ± 0.05nm for ZnO films grown on Si(1 1 1) and Si(1 0 0) orientation, respectively.

Acknowledgements

Financial support from FRGS grant and Universiti Sains Malaysia are gratefully acknowledged.

References

[1] Z. L.Wang, J. Phys. Condens. Matter **16**, R829 (2004).
[2] B. Q. Cao, W. P. Cai, Y. Li, F. Q. Sun, L. D. Zhang, Nanotechnology **16,** 1734 (2005).
[3] Y. H. Leung, A. B. Djuriˇsic´, J. Gao, M. H. Xie, Z. F. Wei, S. J. Xu,W. K. Chan, Chem. Phys. Lett. **394**, 452 (2004).
[4] Z. L. Wang, Annu. Rev. Phys. Chem. **55**, 159 (2004).
[5] J. D. Holladay, Y. Wang, E. Jones, Chem. Rev. **104**, 4767 (2004).
[6] K. G. Saw, Y. T. Lim, G. L. Tan, Z. Hassan, K. Ibrahim, F. K. Yam, S. S. Ng, Journal of Phys. D: Appl. Phys. **41**, 055506 (2008).
[7] G. C. Yi, C. R.Wang, W. I. Park, Semicond. Sci. Technol. **20**, S22 (2005).
[8] J. H. Yang, J. H. Lang, L. L. Yang, Y. J. Zhang, D. D. Wang, H. G. Fan, H. L. Liu, Y. X. Wang, M. Gao, J. Alloys Compd. **450**, 521 (2008).
[9] C. C. Tang, S. S. Fan, M. L. Chapelle, P. Li, Chem. Phys. Lett. **333**, 12 (2001).
[10] D. D. Wang, J. H. Yang, L. L. Yang, Y. J. Zhang, J. H. Lang, M. Gao, Cryst. Res. Technol. **43**, 1041 (2008).
[11] L. C. Nistor, C. Ghica, D. Matei, G. Dinescu, M. Dinescu, G. Van Tendeloo, J. Cryst. Growth **277**(1–4), 26 (2005).
[12] X. T. Zhang, Y. C. Liu, Z. Z. Zhi, J. Y. Zhang, Y. M. Lu, W. Xu, D. Z. Shen, G. Z. , X. W. Fan, X. G. Kong, J. Cryst. Growth **240**, 463 (2002).
[13] Y. Zhang, B. X. Lin, Z. X. Fu, C. H. Liu,W. Han, Opt. Mater. **28,** 1192 (2006).
[14] M. Guo, P. Diao, S. M. Cai, Appl. Surf. Sci. **249**, 71 (2005).
[15] C. Y. Leung, A. B. Djurisic, Y. H. Leung, L. Ding, C. L. Yang, W. K. Ge, J. Cryst. Growth **290,** 131 (2006).
[16] S. P. Chang, S. J. Chang, Y. Z. Chiou, C. Y. Lu, T. K. Lin, C. F. Kuo, H. M. Chang, U. H. Liaw, J. Crystal Growth **310**, (2902008).
[17] L. S. Chuah, Z. Hassan, S. S. Ng, H. Abu Hassan, J. of Alloys and Compounds **479**, L54 (2009).
[18] V. S. Y. Lin, K. Motesharei, K. P. S. Dancil, M. J. Sailor, M. R. Ghadiri, Science **278,** 840 (1997).
[19] X. Li, Y-W. Kim, P. W. Bohn, I. Adesida, Appl. Phys. Lett. **20**, 980 (2002).
[20] M. A. Steven-Kaleeff, I. M. Tiginyanu, S. Langa, H. Foll, H. L. Hartnagel, J. Appl. Phys. **89,** 2560 (2001).
[21] M. Mynbaeva, N. Bazhenov, K. Mynbaev, E. Evstropov, S. E. Saddow, Y. Koshka, Y. Melnik, Phys. Status Solidi B, **228,** 589 (2001).
[22] L. S. Chuah, Z. Hassan, F. K. Yam, H. Abu Hassan, Surface Review and Letters **16**(1), 93 (2009).
[23] J. H. Yang, J. H. Zheng, H. J. Zhai, L. L. Yang, Cryst. Res, Technol. **44**(1), 87 (2009).

*Corresponding author : chuahleesiang@yahoo.com